ACS Chemical Neuroscience
Research Article
Cite This: ACS Chem. Neurosci. 2018, 9, 2554−2562
pubs.acs.org/chemneuro

Hyperpolarized ^{13}C Magnetic Resonance Spectroscopy Reveals the Rate-Limiting Role of the Blood−Brain Barrier in the Cerebral Uptake and Metabolism of L-Lactate *in Vivo*

Yuhei Takado,[†,‡] Tian Cheng,[§] Jessica A. M. Bastiaansen,[∥,⊥] Hikari A. I. Yoshihara,[†] Bernard Lanz,[#] Mor Mishkovsky,[∥] Sylvain Lengacher,[@] and Arnaud Comment*[,†,▽]

[†]Institute of Physics of Biological Systems, Ecole Polytechnique Fédérale de Lausanne, CH-1015 Lausanne, Switzerland
[‡]Department of Functional Brain Imaging Research, National Institutes for Quantum and Radiological Science and Technology, Chiba, Japan
[§]Cancer Research UK Cambridge Institute, University of Cambridge, Li Ka Shing Centre, Cambridge, United Kingdom
[∥]Laboratory of Functional and Metabolic Imaging, Ecole Polytechnique Fédérale de Lausanne, CH-1015 Lausanne, Switzerland
[⊥]Department of Radiology, University Hospital Lausanne (CHUV) and University of Lausanne (UNIL), Lausanne, Switzerland
[#]Sir Peter Mansfield Magnetic Resonance Center, The University of Nottingham, Nottingham NG7 2RD, United Kingdom
[@]Laboratory of Neuroenergetics and Cellular Dynamics, Ecole Polytechnique Fédérale de Lausanne, CH-1015 Lausanne, Switzerland
[▽]General Electric Healthcare, Chalfont St Giles, Buckinghamshire HP8 4SP, United Kingdom

Supporting Information

ABSTRACT: The dynamics of L-lactate transport across the blood−brain barrier (BBB) and its cerebral metabolism are still subject to debate. We studied lactate uptake and intracellular metabolism in the mouse brain using hyperpolarized ^{13}C magnetic resonance spectroscopy (MRS). Following the intravenous injection of hyperpolarized [1-^{13}C]lactate, we observed that the distribution of the ^{13}C label between lactate and pyruvate, which has been shown to be representative of their pool size ratio, is different in NMRI and C57BL/6 mice, the latter exhibiting a higher level of cerebral lactate dehydrogenase A (*Ldha*) expression. On the basis of this observation, and an additional set of experiments showing that the cerebral conversion of [1-^{13}C]lactate to [1-^{13}C]pyruvate increases after exposing the brain to ultrasound irradiation that reversibly opens the BBB, we concluded that lactate transport is rate-limited by the BBB, with a 30% increase in lactate uptake after its disruption. It was also deduced from these results that hyperpolarized ^{13}C MRS can be used to detect a variation in cerebral lactate uptake of <40 nmol in a healthy brain during an *in vivo* experiment lasting only 75 s, opening new opportunities to study the role of lactate in brain metabolism.

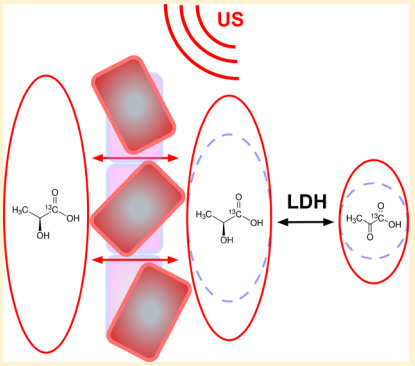

KEYWORDS: *Hyperpolarization, magnetic resonance spectroscopy, dynamic nuclear polarization, ultrasound, pyruvate, bicarbonate*

INTRODUCTION

The role of lactate as a source of energy for the mammalian brain has repeatedly been a subject of debate,[1−3] but it is established that the level of utilization of lactate by the brain increases with an increase in the lactate plasma concentration following lactate injection or exercise. While glucose is thought to be preferentially taken up by astrocytes,[4] a large number of observations show that lactate is predominantly taken up by neurons and transformed, via lactate dehydrogenase (LDH), into pyruvate for mitochondrial oxidation.[5] In mice, it has been demonstrated that lactate is metabolized by the intact brain in an activity-dependent manner.[3]

L-Lactate can cross the blood−brain barrier (BBB) relatively easily and is taken up by cells in the mammalian brain either via monocarboxylate transporters (MCTs) in the plasma membrane or by nonsaturable diffusion.[6] There is an equilibration between blood and brain concentrations,[1,7] and at high plasma lactate levels, the transport is dominated by nonfacilitated mechanisms.[8] Earlier studies in rats[9] and in patients[10] had shown that this equilibration is not immediate, leaving unsettled the question of the kinetics of transport of lactate through the BBB. After its uptake into brain cells, lactate rapidly equilibrates with pyruvate through the action of LDH. The conversion is a near-equilibrium reaction governed by the relation $[\text{pyruvate}]/[\text{lactate}] = K_{\text{LDH}}[\text{NAD}^+]/([\text{NADH}][\text{H}^+])$, where K_{LDH} is the equilibrium constant for lactate dehydrogenase.

Received: February 12, 2018
Accepted: May 17, 2018
Published: May 17, 2018

DOI: 10.1021/acschemneuro.8b00066
ACS Chem. Neurosci. 2018, 9, 2554−2562

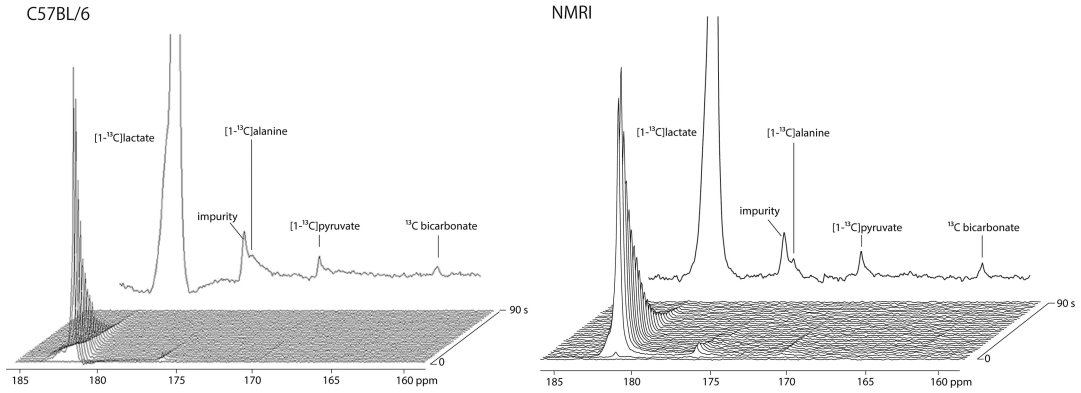

Figure 1. Representative dynamic ^{13}C MRS spectra measured in a C57BL/6 mouse (left) and a NMRI mouse (right) head following the injection of hyperpolarized [1-^{13}C]lactate. Along with the substrate resonance at 183 ppm, the three expected metabolites were detected: [1-^{13}C]pyruvate at 171 ppm, [^{13}C]bicarbonate at 161 ppm, and [1-^{13}C]alanine at 176 ppm (overlapping with an impurity peak). The delay between each acquisition was set to 3 s, starting 2 s after the beginning of the injection. A sum of spectra 2−26 is shown at the top.

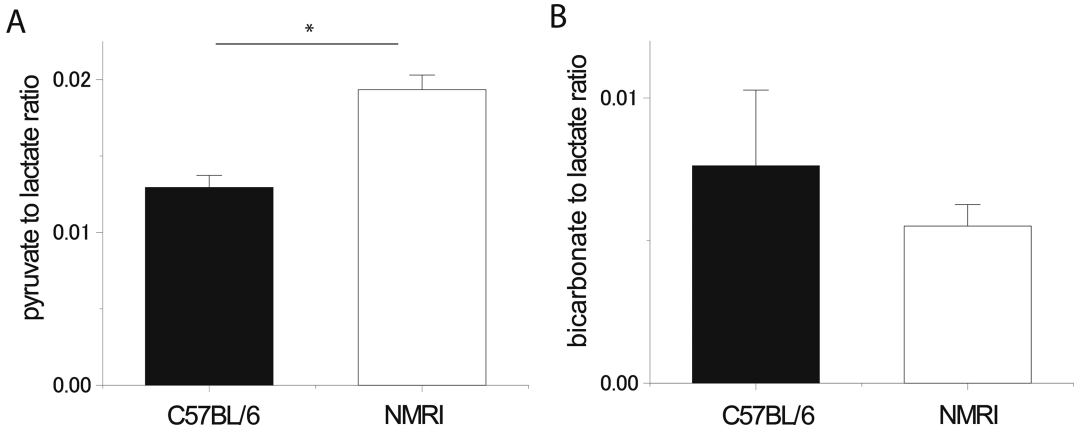

Figure 2. (A) Pyruvate-to-lactate ratio deduced from the hyperpolarized ^{13}C MRS experiments (sum of spectra 2−26) performed in two different mice strains (C57BL/6 and NMRI). The ratio is significantly different for the two groups ($p < 0.05$). (B) Bicarbonate-to-lactate ratio deduced from the same experiments and for the two groups. The difference was not significant. Error bars represent the mean ± the standard error of the mean (SEM).

^{13}C magnetic resonance spectroscopy (MRS) has been widely used to investigate the kinetics of substrate utilization in cerebral intermediary metabolism, in particular following the fate of infused [^{13}C]glucose and [^{13}C]lactate. However, this technique is limited by poor sensitivity, which precludes directly probing metabolic transformations taking place within the first minute of injection. With the advent of dissolution dynamic nuclear polarization (DNP),[11] hyperpolarized (HP) ^{13}C MRS has become a powerful technique for monitoring fast metabolic conversions *in vivo* by enhancing the sensitivity of MRS signals by ≤4 orders of magnitude.[12] It is assumed that the lactate-to-pyruvate ratio derived from hyperpolarized [^{13}C]pyruvate can be a suitable marker of LDH activity.[13−15] Studies using hyperpolarized [^{13}C]pyruvate have also shown that the limited transport of pyruvate across the BBB can be a significant constraint for cerebral metabolic studies based on hyperpolarized ^{13}C MRS.[16]

Several recent studies have shown that hyperpolarized [^{13}C]lactate can also be used to investigate lactate-to-pyruvate conversion *in vivo*.[17−22] Compared to pyruvate, hyperpolarized lactate has the advantage that a bolus injection does not greatly alter its circulating concentration, because lactate has a physiological concentration substantially higher than that of pyruvate in the blood.[23]

It has previously been demonstrated that the [^{13}C]lactate signal detected *in vivo* following the injection of hyperpolarized [^{13}C]pyruvate mostly originates from the rapid ^{13}C label exchange catalyzed by LDH and that the net production of lactate is nearly negligible.[24,25] The intensity of the lactate signal is therefore expected to be directly related to the endogenous lactate pool size, and this property can be used to detect tumorous tissue, which is known to have a lactate concentration higher than that of healthy tissue.[26] The same holds true for the [^{13}C]pyruvate signal measured following the injection of hyperpolarized [^{13}C]lactate, the intracellular pyruvate pool being labeled by exchange catalyzed by LDH.[20] With both hyperpolarized ^{13}C-labeled substrates, the detected pyruvate-to-lactate ^{13}C signal ratio is representative of the local pyruvate-to-lactate concentration ratio because LDH governs the equilibrium between these two metabolites.

The aim of this study was to evaluate the rate-limiting role of the BBB on equilibration between the plasma and brain within the first minute following the intravenous injection of hyperpolarized [1-^{13}C]lactate. We first established that the kinetics of the observed cerebral [1-^{13}C]pyruvate signal can provide a measure of cerebral [1-^{13}C]lactate uptake through its rapid intracellular equilibration catalyzed by LDH, by performing hyperpolarized ^{13}C MRS experiments in two mouse strains,

DOI: 10.1021/acschemneuro.8b00066
ACS Chem. Neurosci. 2018, 9, 2554−2562

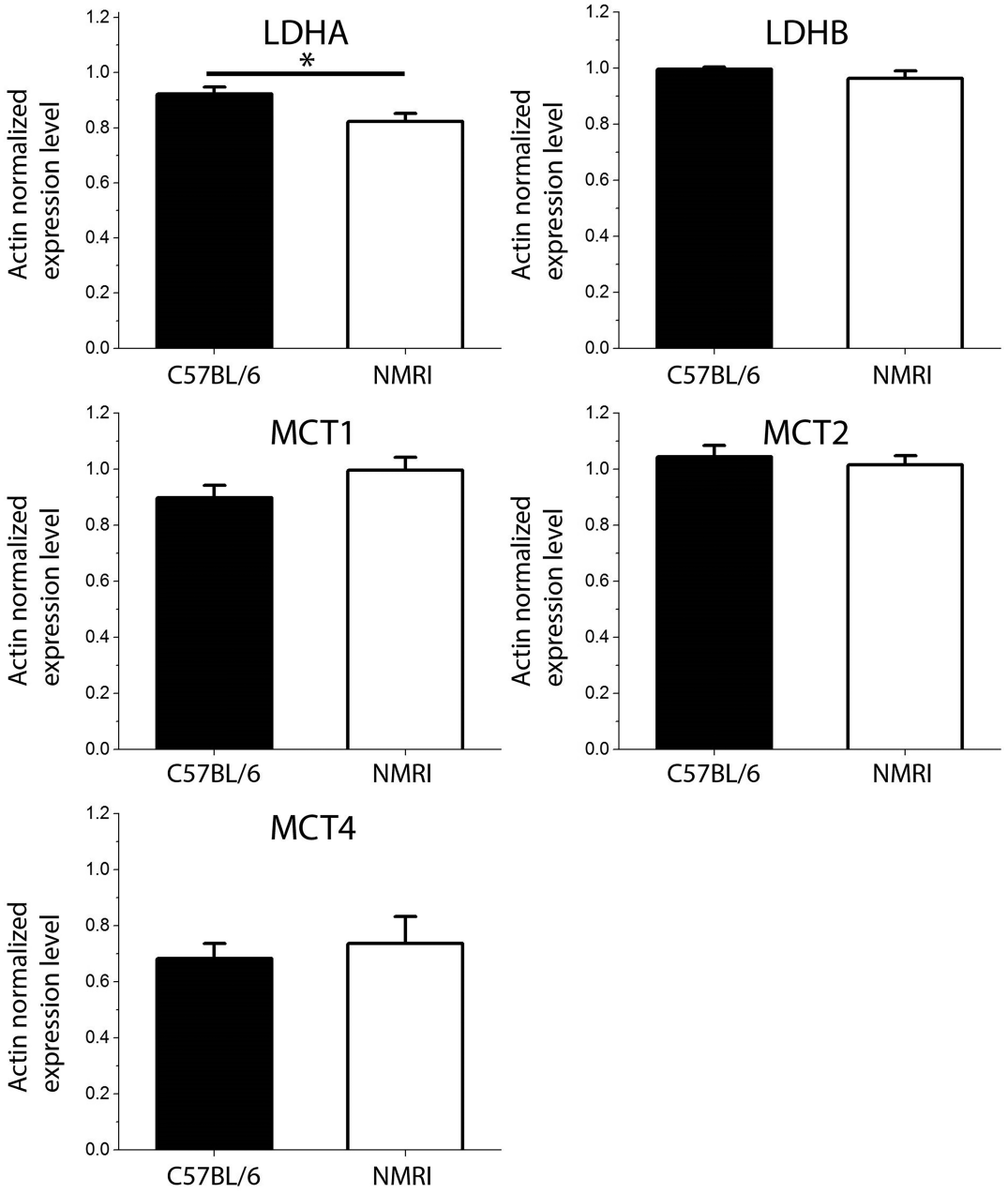

Figure 3. Quantitative PCR data for C57BL/6 (n = 7) and NMRI (n = 7) mice. Only the *Ldha* expression level was significantly different between C57BL/6 and NMRI mice brain (p = 0.025).

namely, C57BL/6 and NMRI, that exhibit differences in *Ldha* expression. The rate-limiting role of the BBB in lactate transport was then assessed by disrupting the BBB with ultrasound and microbubbles, following a protocol described previously.[27]

RESULTS AND DISCUSSION

The hyperpolarized ^{13}C magnetic resonance (MR) signals originating from the injected substrate, [1-^{13}C]lactate (183 ppm), and its metabolites, [1-^{13}C]alanine (176 ppm) and [1-^{13}C]pyruvate (171 ppm), were detected in all the experiments (n = 19) (Figure 1). [^{13}C]Bicarbonate (161 ppm) was also observed in nearly all the experiments (18 of 19). The additional peak observed around 176.5 ppm corresponds to an impurity overlapping with the [1-^{13}C]alanine peak and was confirmed by high-resolution ^{13}C nuclear magnetic resonance (NMR) of the purchased solution (data not shown). Compared to that of NMRI mice, the pyruvate-to-lactate ratio was clearly smaller in C57BL/6 mice (p < 0.05), while the bicarbonate-to-lactate ratio was not significantly different between the two strains (Figure 2).

The origin of the higher pyruvate-to-lactate signal ratio observed in NMRI mice as compared to C57BL/6 mice could possibly be a difference in cerebral MCTs between the two strains. The quantitative real-time polymerase chain reaction (PCR) analyses did however not exhibit any significant difference in *Mct* expression (Figure 3). Because MCT activity was not measured, it is nevertheless not possible to completely rule out the possibility that a difference in cerebral MCTs may have had an impact on the observed pyruvate-to-lactate signal ratios. The results of the quantitative real-time PCR analyses highlighted that the level of *Ldha* expression in NMRI mice

DOI: 10.1021/acschemneuro.8b00066
ACS Chem. Neurosci. 2018, 9, 2554−2562

brain was lower than in C57BL/6 mice ($p < 0.05$), while no significant difference was found in *Ldhb* expression between the two strains (Figure 3). It was previously proposed that an increased level of expression of *Ldha* might lead to an increased lactate concentration in the brain.[28,29] Although the p value did not reach the level of significance, it was also previously observed in a ^{1}H MRS study that C57BL/6 mice have a lactate brain concentration higher than that of NMRI mice.[30]

These observations coupled to the fact that no significant difference in blood lactate concentration was found between C57BL/6 (1.1 ± 0.2 mM) and NMRI (1 ± 0.1 mM) led us to the conclusion that the variation in the pyruvate-to-lactate ratio is most likely not due to a difference in transport kinetics but rather a reflection of the endogenous lactate pool size. Our observation therefore seems to be a confirmation that the pyruvate-to-lactate signal ratio is correlated to the ratio between the two metabolite pool sizes and shows that it is possible to determine variations in lactate pool size using hyperpolarized [1-^{13}C]lactate. Because the detected pyruvate signal originates from cerebral tissue only and we did not observe any difference in lactate blood concentration between the two strains, we could conclude that our observation is related to unequal intracellular concentrations.

To assess the role of the BBB on the kinetics of transport of L-lactate into the brain, we measured the cerebral pyruvate signal pre- and post-ultrasound irradiation. The analysis is based on the assumption that LDH will nearly instantaneously equilibrate the distribution of ^{13}C between the two pools as soon as lactate has entered the brain. This assumption is reasonable given that the transport kinetics across the BBB is at least 1 order of magnitude slower than the apparent rate constant associated with intracellular transport and LDH activity in the rodent brain.[16,31] Because the pyruvate-to-lactate ratio determined from our measurements was larger in NMRI mice than in C57BL/6 mice, the study was performed on the former strain. To assess the effect of ultrasound on the BBB, T_1-weighted images of the brain were acquired in NMRI mice after administration of either Gd^{3+} (Figure S1) or Mn^{2+} (Figure S2). The striking change in contrast observed in the images, particularly in the lateral ventricles that exhibit a hyperintense signal following ultrasound irradiation, confirmed the opening of the BBB after the injection of microbubbles and the application of ultrasound.

To quantify the increase in the intracellular cerebral lactate concentration after ultrasound application, we propose the following model illustrated in Figure 4. In the absence of ultrasound (US) exposure, the pyruvate-to-lactate ^{13}C signal ratio can be written as follows

$$\left|\frac{S_{pyr}}{S_{lac}}\right|_{NoUS} = \frac{S_{pyr}^{brain}}{S_{lac}^{blood} + S_{lac}^{brain}} \quad (1)$$

where the [1-^{13}C]pyruvate signal (S_{pyr}^{brain}) originates exclusively from the brain cells. If we assume that the ^{13}C fractional enrichments for both pyruvate and lactate brain pools are equal because of the rapid exchange through LDH

$$\left|\frac{S_{pyr}}{S_{lac}}\right|_{NoUS} = \frac{S_{lac}^{brain}\frac{[pyr]}{[lac]}}{S_{lac}^{blood} + S_{lac}^{brain}} \quad (2)$$

where [pyr] and [lac] are the pyruvate and lactate brain concentrations, respectively. When the brain is exposed to ultrasound irradiation, S_{lac}^{brain} can be replaced by $S_{lac}^{brain}(1 + \delta)$,

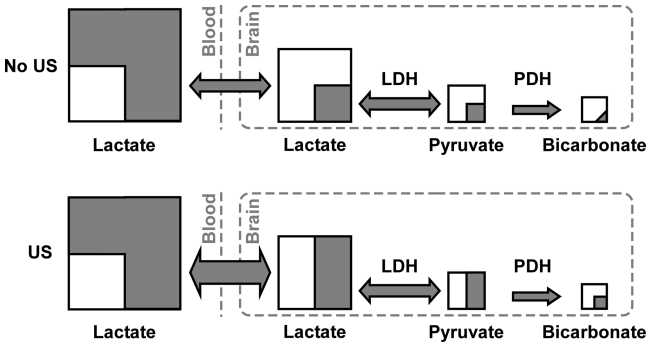

Figure 4. Schematic representation of the ^{13}C label distribution, across the detected metabolites in the mouse brain exposed to ultrasound (US, bottom) and not exposed to US (top), 75 s after the intravenous injection of [1-^{13}C]lactate. Each square represents a metabolic pool, with the gray part corresponding to the ^{13}C-labeled fraction. The gray arrows represent the ^{13}C label flux between the pools. Note that the relative size of the squares or the gray area within each pool is not scaled to the real pool size ratios or the proportion of the ^{13}C label.

where δ is the portion of the ^{13}C signal originating from the increase in brain lactate concentration during the measurement. We obtain

$$\left|\frac{S_{pyr}}{S_{lac}}\right|_{US} = \frac{S_{lac}^{brain}(1 + \delta)\frac{[pyr]}{[lac]}}{S_{lac}^{blood} + S_{lac}^{brain}} \quad (3)$$

where S_{lac}^{blood} is assumed to be identical in both cases because the decrease in blood lactate concentration due to higher cerebral uptake is negligible and $S_{lac}^{blood} + S_{lac}^{brain} \gg \delta S_{lac}^{brain}$ to approximate the denominator from $S_{lac}^{blood} + S_{lac}^{brain}(1 + \delta)$ to $S_{lac}^{blood} + S_{lac}^{brain}$. Therefore, the change in ^{13}C signal ratio induced by the application of ultrasound is reduced to

$$\left|\frac{S_{pyr}}{S_{lac}}\right|_{US} = \left|\frac{S_{pyr}}{S_{lac}}\right|_{NoUS} \times (1 + \delta) \quad (4)$$

The pyruvate-to-lactate ratio measured in mice exposed to ultrasound irradiation was significantly higher than that in mice that did not experience ultrasound exposure (Figure 5). The 28 ± 3% increase ($p < 0.05$) post-ultrasound demonstrates that the BBB limits the transport of lactate into the brain. Although the difference in the bicarbonate-to-lactate ratio did not quite reach the level of significance ($p = 0.45$), most likely because of the low SNR, the observed trend toward increased conversion also points in the direction of an increased lactate transport rate post-ultrasound.

It has been shown that the intracellular and extracellular hyperpolarized [1-^{13}C]lactate signals can be separated *in vitro*.[32] It was however not possible to achieve the required spectral resolution in the *in vivo* study presented here. As a consequence, we could not deduce the Michaelis–Menten constants associated with BBB transport. However, because of the rapid exchange catalyzed by LDH, the detection of cerebral pyruvate provides an indirect readout of the transport of lactate into the brain. In fact, the increase in the pyruvate-to-lactate ratio following ultrasound irradiation corresponds to a quantitative measurement of the increased cerebral lactate uptake, δ (see eq 4). We conclude that the application of ultrasound led to an increase of 28 ± 3% of cerebral lactate within the 75 s experiment. It was previously demonstrated that lactate flux through the BBB via nonfacilitated transport is

DOI: 10.1021/acschemneuro.8b00066
ACS Chem. Neurosci. 2018, 9, 2554–2562

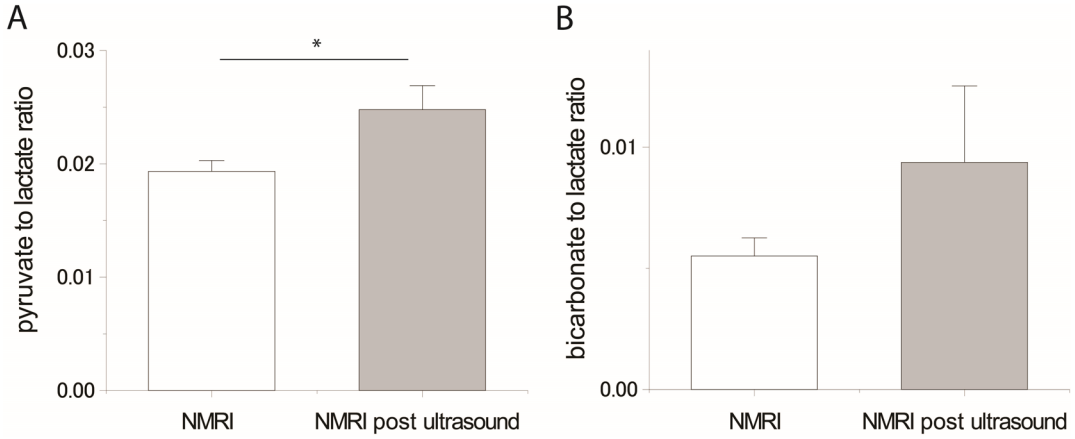

Figure 5. (A) Pyruvate-to-lactate ratio deduced from the hyperpolarized ^{13}C MRS experiments (sum of spectra 2−26) performed in NMRI mice with or without ultrasound irradiation. The ratio is significantly different for the two groups ($p < 0.05$). (B) Bicarbonate-to-lactate ratio deduced from the same experiments and for the two groups. The differences were not significant. Error bars represent the mean ± the standard error of the mean.

roughly identical to the flux via MCTs in the rat brain across a large lactate plasma concentration range.[33] Assuming the uptake via MCTs was not substantially affected by ultrasound, nonfacilitated transport would then account for the nearly 30% increase in lactate uptake after opening the BBB. Note that because the pyruvate and bicarbonate signals originate from the intracellular compartment, their intensity will not be affected by a potential variation in extracellular pH that may result from the opening of the BBB.

Using a V_{max} of 300 nmol g^{-1} min^{-1} and a K_M of 13 mM as the Michaelis−Menten constants for the kinetics of transport of lactate across the BBB,[8] we estimate for a 700 mg mouse brain (42 g body weight corresponds to 0.017 × 42 = 0.7 g brain weight for a male[34]), with 13 mM lactate in the blood, that approximately 150 × 0.7 × 75/60 = 130 nmol of lactate entered the brain during the 75 s experiment. This is consistent with the results obtained in NMRI mice using thermally polarized [3-^{13}C]lactate, where 516 nmol was estimated to be taken up by the brain within 5 min of a bolus injection (with a lactate dose nearly 5-fold larger than that in the study presented here).[35] It can therefore be concluded that the method herein presented allows for the detection of a 130 × 0.28 ≅ 36 nmol increase in lactate uptake upon BBB opening by ultrasound, demonstrating the high sensitivity of hyperpolarized ^{13}C MRS in studying cerebral metabolism.[36] For future hyperpolarized ^{13}C MR imaging studies aiming at correlating the spatiotemporal evolution of the BBB opening with hyperpolarized ^{13}C MRI, it would be necessary to determine the spatiotemporal delivery of small molecules like [^{13}C]lactate as was done by Choi et al. with Gd-based contrast agents.[37]

The dynamics of transport of a substrate across the BBB has previously been studied using hyperpolarized ^{13}C MR. Hurd et al. looked at the cerebral metabolism of [1-^{13}C]pyruvate[16] and ethyl [1-^{13}C]pyruvate.[31] Because the flux through MCTs is on the order of 4 times slower for pyruvate than for lactate,[38] and the pyruvate plasma concentration largely exceeded K_M, it can be assumed that MCTs were saturated following the injection of hyperpolarized [^{13}C]pyruvate. Consequently, the non-saturable flux could be considered as the main contribution to transport across the BBB, but the more hydrophobic precursor ethyl [1-^{13}C]pyruvate crossed the BBB much faster and resulted in greater cerebral [1-^{13}C]lactate production. Although the results of this previous study are highly important in the context of hyperpolarized ^{13}C MR because [^{13}C]pyruvate is by far the most widely used substrate and to date the only one used in humans, the authors highlighted that the contribution of extracellular [^{13}C]lactate to the measured brain signal is difficult to estimate. For this reason, injecting hyperpolarized [^{13}C]lactate is an interesting alternative because the signal from its metabolic product pyruvate is purely intracellular. In fact, both pyruvate and lactate concentrations stay near physiological range following the injection of a bolus of hyperpolarized [^{13}C]lactate. The disadvantages of using hyperpolarized [^{13}C]lactate are that the fractional ^{13}C enrichment of brain lactate during the time frame of the experiment is limited and the pool size of pyruvate is small, leading to a sensitivity lower than that in experiments performed with hyperpolarized [^{13}C]pyruvate. It is however worth noting that the bicarbonate signal intensity is not substantially higher in experiments with hyperpolarized [^{13}C]pyruvate with a similar ^{13}C polarization level using the same equipment.[39] It can also be mentioned here that the use of sodium lactate instead of lactic acid, which is considerably less stable, greatly simplifies sample preparation and precludes the need for adding sodium hydroxide to reach physiological pH in the hyperpolarized [^{13}C]lactate solution prior to injection. Note finally that alternative hyperpolarized ^{13}C MR approaches based on flow,[40] chemical shift,[32,41] and diffusion weighting measurements[42,43] could be used to study the impact of ultrasound on the dynamics of transport of small molecules across the BBB.

CONCLUSION

We demonstrated that transport of L-lactate across the BBB can be observed using hyperpolarized [^{13}C]lactate, and we deduced that its transport is limited by the BBB. Our findings show that the equilibration between plasma and brain lactate is not instantaneous and that the BBB can restrict diffusion into the brain by nearly 30% at high plasma lactate concentrations. We also deduced that, although an exact determination of metabolite concentrations is challenging using hyperpolarized ^{13}C, variations of <40 nmol in cerebral lactate uptake can be detected. Our study shows that [1-^{13}C]lactate is a promising molecule for studying cerebral metabolism by hyperpolarized ^{13}C MRS because the injected substrate and its metabolites,

DOI: 10.1021/acschemneuro.8b00066
ACS Chem. Neurosci. 2018, 9, 2554−2562

namely, pyruvate and bicarbonate, remain and can be detected at near physiological concentrations. Hyperpolarized [^{13}C]-lactate could also be potentially considered as a nontoxic alternative to lanthanide-based contrast agents for diagnosing brain tumors through the evaluation of BBB integrity by MRI.

METHODS

All experiments were conducted in accordance with the Animal Research: Reporting of In Vivo Experiments (ARRIVE) guidelines and were approved by the local regulatory body of the Canton Vaud, Switzerland (Service de la consommation et des affaires vétérinaires, Affaires vétérinaires, Canton de Vaud, Switzerland). All animals were purchased from Charles River Laboratories (Châtillon-sur-Chalaronne, France).

Animal Preparation and Injection Protocol. A total of seven C57BL/6J mice (29.1 ± 1.5 g, 10−24 weeks of age, male) and 17 NMRI mice (41.7 ± 1.4 g, 10−24 weeks of age, male) were purchased for the MR experiments. All mice were anesthetized using 1.5−2% isoflurane in air containing 50% oxygen (1 L/min). A 12 cm long homemade catheter was introduced into the femoral vein 60 min before each hyperpolarized ^{13}C MRS experiment. Animal physiology, e.g., body temperature and respiration rate, was monitored and kept stable during the experiments by controlling the temperature of circulating warm water and the amount of isoflurane delivered to the animal. The animals were euthanized in accordance with local guidelines at the end of each hyperpolarized ^{13}C MRS experiment.

Preparation of the Hyperpolarized [1-^{13}C]Lactate Solution. A mixture of a sodium [1-^{13}C]lactate solution [45−55% (w/w) in H_2O, 99 atom % ^{13}C] and d_8-glycerol [1:1 (w/w)] doped with 50 mM 4-hydroxy-2,2,6,6-tetramethylpiperidin-1-oxyl (TEMPOL) radical was warmed for 15 min in a water bath at 50 °C.[17−22] All chemicals were purchased from Sigma-Aldrich (Buchs, Switzerland). A total volume of 0.2 mL of 2 ± 0.5 μL frozen beads was prepared in liquid nitrogen and placed into a polytetrafluoroethylene (PTFE) sample cup described in a previous publication.[44] The cup was then loaded into a 5 T home-built DNP polarizer and polarized at 1 ± 0.05 K and 140.18 GHz with a millimeter-wave power output of 50 mW.[45] The solid-state ^{13}C polarization buildup was monitored by applying a 5° radiofrequency (rf) pulse every 5 min.

***In Vivo* Hyperpolarized ^{13}C MRS.** All *in vivo* MR acquisitions were performed with a Direct Drive spectrometer (Agilent, Palo Alto, CA) interfaced to an actively shielded 9.4 T magnet with a 31 cm horizontal bore (Magnex Scientific, Abingdon, U.K.) using a home-built dual-channel surface coil consisting of 12 mm diameter quadrature ^{1}H loops and an 8 mm diameter ^{13}C surface coil. After the animal had been positioned inside the magnet, series of axial, sagittal, and coronal two-dimensional images were acquired using a gradient echo sequence (TR = 50 ms, TE = 3 ms, field of view = 30 × 30 mm, matrix = 128 × 128, flip angle = 30°) from which the volume of interest (VOI) was selected. The static magnetic field was shimmed in a 75 μL (3 mm × 5 mm × 5 mm) voxel to reduce the localized proton line width to 20 Hz using the FAST(EST)MAP protocol.[46]

After being polarized for 2 h, the frozen beads were rapidly dissolved in 6 mL of superheated D_2O and transferred into the separator/infusion pump,[44,47] which was located inside the magnet bore, over 2 s. A ^{13}C polarization of 10 ± 2% was measured at the time of injection inside the pump as described in a previous publication.[47] The concentration of the infusate, measured afterward in a high-resolution NMR system, was 110 ± 20 mM. Either 200 μL (for seven C57BL/6 mice) or 300 μL (for 12 NMRI mice) of a hyperpolarized [1-^{13}C]lactate solution was injected within 5 s, corresponding to a volume-to-weight ratio of ∼7 μL/g. The blood concentration at the end of the injection was estimated to be 13 ± 3 mM. Starting 5 s after dissolution, 40 single-pulse ^{13}C acquisitions were sequentially recorded every 3 s using 30° adiabatic rf pulses (BIR4) with ^{1}H decoupling during acquisition (WALTZ-16). Localization was achieved by placing the surface coil on top of the mouse head. The adiabatic pulse offset and power were set to ensure a homogeneous 30° excitation of substrate and metabolite resonances within the entire VOI.

After induction of the BBB opening in NMRI mice, hyperpolarized [1-^{13}C]lactate was injected using the same protocol that was used without ultrasound application.

Quantitative Real-Time PCR Analysis and Blood Lactate Measurement. A set of seven C57BL/6J mice (28.4 ± 0.5 g, 10 weeks of age, male) and seven NMRI mice (42.4 ± 1.0 g, 10 weeks of age, male) were subjected to PCR analyses. Quantitative real-time PCR was performed to measure the expression levels of *Ldha*, *Ldhb*, *Slc16a1* (MCT1), *Slc16a7* (MCT2), and *Slc16a3* (MCT4) transcripts associated with the metabolism of [1-^{13}C]lactate for both C57BL/6 mice and NMRI mice. The plasma lactate concentration was measured with the lactate oxidase method using a multiassay analyzer (GW7Micro-Stat, Analox Instruments, London, U.K.). For the quantitative PCR measure, mice were rapidly killed with a guillotine and brains extracted; 40 mg of brain cortex was directly mixed in a lysis solution. RNA was extracted using the Maxwell 16 LEV simplyRNA Cells kit (Promega, ref AS1270) following the manufacturer's instructions. Reverse transcriptions were performed with the High Capacity RNA-to-cDNA Kit (Life Technologies) according to the manufacturer's instructions. Each reaction was performed in a volume of 20 μL with 400 ng of mRNA. Quantitative determination of the targeted mRNA sequences was performed with the fast real-time PCR Applied Biosystem 7900HT system (Applied Biosystens, Rotkreuz, Switzerland). The following primers (5′−3′) were used: mActinBF031, GCT TCT TTG CAG CTC CTT CGT; mActinbRE94, ATA TCG TCA TCC ATG GCG AAC; mLDHAFo427, TTG TCT CCA GCA AAG ACT ACT GTG T; mLDHARe536, TTT CGC TGG ACC AGG TTG AG; mLDHBFo312, GCA GCA CGG GAG CTT GTT; mLDHBRe389, CAA TCT TAG AGT TGG CTG TCA CAG A; mMCT1Fo1361, AAT GCT GCC CTG TCC TCC TA; mMCT1Re1441, CCC AGT ACG TGT ATT TGT AGT CTC CAT; mMCT2Fo755, CAG CAA CAG CGT GAT AGA GCT T; mMCT2Re830, TGG TTG CAG GTT GAA TGC TAA T; mMCT4Fo320, TCT GCA GAA GCA TTA TCC AGA TCT A; mMCT4Re407, ATG ATG AGG GAA GGC TGG AA. Gene expression data were analyzed using an Excel macro from Frontiers in Genetics (RT-PCR analysis-macro version 1.1). The average quantities were normalized to a normalization factor obtained by calculating the geometric mean of the most stable reference gene.[48] For the normalization factor, we tested the β-actin, cyclophilin, hypoxanthine guanine phosphoribosyl transferase, and TATA box binding protein genes and chose β-actin as it was the most stable gene in our study.

Protocol for BBB Opening. The BBB was opened using a previously described method.[49] In brief, a circular single-element ultrasound transducer (model A306S-SU, Olympus NDT) with a diameter of 13 mm and a center frequency of 2.25 MHz was used in this study. Using a stereotaxic instrument, the transducer was positioned at its natural focal distance (58 mm) in a column of degassed water (contained by a thin plastic film) placed directly over the mouse brain. The transducer was driven by a 47 dB power amplifier (model RF0510-200, RFPA), which was fed by a periodic pulse sequence from a signal generator (model 33220A, Agilent, Santa Clara, CA). The pulse sequence consisted of bursts of 2.15 MHz sinusoidal pulses with 50000 cycles per burst and a burst period of 64 ms. The pulse amplitude was calibrated to generate negative acoustic pressure peaks of 0.5 MPa at the center of the natural focus of the transducer. The power output of the ultrasonic transducer was calibrated in a water bath using a needle hydrophone (1 mm diameter needle hydrophone probe containing a 28 μm thick gold electroded polyvinylidene fluoride film, Precision Acoustics Ltd.).

Prior to the application of ultrasonic excitation, hair was removed from the mouse scalp using an electric trimmer. Ultrasound gel was placed on the scalp, and the water column was lowered onto the head. A 100 μL bolus of sulfur hexafluoride microbubbles with a phospholipid shell (SonoVue, Bracco Imaging, Milan, Italy) was administered through the femoral vein within 5 s, ∼1 min before ultrasound irradiation. Following microbubble injection, the ultrasound pulse sequence was initiated and maintained for 10 min. Note that to ensure an effective opening of the BBB, we applied a pulse

DOI: 10.1021/acschemneuro.8b00066
ACS Chem. Neurosci. 2018, 9, 2554−2562

substantially longer (10 min instead of 3 min) than that in the original protocol published by Howles et al.[49] We did however not specifically quantify skull attenuation in this study, but it was previously demonstrated that the opening of the BBB in mice can be induced with ultrasound without craniotomy by compensating for the ∼20% attenuation in pressure amplitude.[50]

The efficacy of the protocol to open the BBB was evaluated via T_1-weighted MRI scans using either a gadolinium-based contrast agent, Gadoteridol (ProHance, Bracco Imaging), injected intraperitoneally 20 min before imaging at a concentration of 2 mmol/kg, or a 100 mM $MnCl_2$ solution (Sigma-Aldrich) injected intraperitoneally 30 min before imaging at a concentration of 0.4 mmol/kg.[51] We used a three-dimensional spoiled gradient-recalled (SPGR) MRI sequence with the following parameters:[49] pulse repetition (TR) = 25 ms, echo time = 6 ms, flip angle = 30°, field of view = 20 × 20 × 16, matrix = 256 × 256 × 32, and number of averages = 4.

Analysis of ^{13}C MRS Data. A nonlinear least-squares quantification algorithm, AMARES, as implemented in the jMRUI software package,[52] was used to fit the ^{13}C MRS data. The spectra were corrected for phase and DC offset. Soft constraints were imposed on peak frequencies (171.0−171.2 ppm for pyruvate, 161.0−161.4 ppm for bicarbonate, and 183.2−183.6 ppm for lactate) and line widths (full width at half-maximum = 10−30 Hz), and the relative phases were fixed to zero. The peak areas of [1-^{13}C]lactate, [1-^{13}C]pyruvate, and [^{13}C]bicarbonate were quantified, averaged over 25 acquisitions (sum of spectra 2−26, corresponding to a total acquisition time of 75 s), and used to compute the pyruvate-to-lactate and bicarbonate-to-lactate ratios. Changes in relative metabolite ratios were used as a measure of kinetic rate changes, because it was previously demonstrated that the kinetic rates obtained from fitting the evolution of the signals of hyperpolarized substrates and its metabolic products are directly proportional to the ratios of the summed spectral signals.[53] The time range was chosen to include only the spectra with a lactate signal-to-noise ratio (SNR) of >2.

Statistics. Statistical analyses were performed using the OriginPro 9.0G software. p values were computed using an unpaired or paired Student's t test, where appropriate. For the statistical analysis of multiple groups, one-way analysis of variance was used followed by Tukey's test. A p value of 0.05 was considered significant. All data are presented as means ± the standard error of the mean unless otherwise stated.

■ ASSOCIATED CONTENT

Supporting Information

The Supporting Information is available free of charge on the ACS Publications website at DOI: 10.1021/acschemneuro.8b00066.

Supplementary figures displaying two sets of T_1-weighted ^{1}H MRI images demonstrating that the BBB was open after the application of ultrasound to the mouse head as described in Methods (PDF)

■ AUTHOR INFORMATION

Corresponding Author

*E-mail: arnaud.comment@ge.com.

ORCID

Arnaud Comment: 0000-0002-8484-3448

Author Contributions

Y.T., M.M., and A.C. designed the study. Y.T., T.C., and J.A.M.B. performed the *in vivo* experiments. Y.T. and H.A.I.Y. analyzed the data. J.A.M.B. and B.L. made a critical contribution to the analysis of the kinetic data. S.L. performed and analyzed the quantitative PCR measurements. A.C. wrote the manuscript. All authors discussed the results and commented on the manuscript.

Funding

This work is part of a project that has received funding from the European Union's Horizon 2020 European Research Council (ERC Consolidator Grant) under Grant Agreement 682574 (ASSIMILES) and was supported by the Swiss National Science Foundation (Grant PP00P2_133562).

Notes

The authors declare the following competing financial interest(s): A.C. is currently employed by General Electric Medical Systems Inc.

■ ACKNOWLEDGMENTS

The authors thank the Centre d'Imagerie BioMédicale (CIBM) of the UNIL, UNIGE, HUG, CHUV, EPFL, and the Leenards and Jeantet Foundations for its support.

■ REFERENCES

(1) Boumezbeur, F., Petersen, K. F., Cline, G. W., Mason, G. F., Behar, K. L., Shulman, G. I., and Rothman, D. L. (2010) The Contribution of Blood Lactate to Brain Energy Metabolism in Humans Measured by Dynamic C-13 Nuclear Magnetic Resonance Spectroscopy. *J. Neurosci. 30*, 13983−13991.

(2) van Hall, G., Strømstad, M., Rasmussen, P., Jans, O., Zaar, M., Gam, C., Quistorff, B., Secher, N. H., and Nielsen, H. B. (2009) Blood lactate is an important energy source for the human brain. *J. Cereb. Blood Flow Metab. 29*, 1121−1129.

(3) Wyss, M. T., Jolivet, R., Buck, A., Magistretti, P. J., and Weber, B. (2011) In vivo evidence for lactate as a neuronal energy source. *J. Neurosci. 31*, 7477−7485.

(4) Jakoby, P., Schmidt, E., Ruminot, I., Gutiérrez, R., Barros, L. F., and Deitmer, J. W. (2014) Higher Transport and Metabolism of Glucose in Astrocytes Compared with Neurons: A Multiphoton Study of Hippocampal and Cerebellar Tissue Slices. *Cereb. Cortex 24*, 222−231.

(5) Bouzier-Sore, A. K., and Pellerin, L. (2013) Unraveling the complex metabolic nature of astrocytes. *Front. Cell. Neurosci. 7*, 179.

(6) Knudsen, G. M., Pettigrew, K. D., Patlak, C. S., and Paulson, O. B. (1994) Blood-Brain-Barrier Permeability Measurements by Double-Indicator Method Using Intravenous-Injection. *Am. J. Physiol. 266*, H987−H999.

(7) Tofteng, F., and Larsen, F. S. (2002) Monitoring extracellular concentrations of lactate, glutamate, and glycerol by in vivo microdialysis in the brain during liver transplantation in acute liver failure. *Liver Transplantation 8*, 302−305.

(8) Knudsen, G. (2012) Blood-Brain Barrier Transport of Lactate. In *Neural Metabolism in Vivo* (Choi, I.-Y., and Gruetter, R., Eds.) pp 755−761, Springer.

(9) Dager, S. R., Marro, K. I., Richards, T. L., and Metzger, G. D. (1992) MRS detection of whole brain lactate rise during 1 m sodium lactate infusion in rats. *Biol. Psychiatry 32*, 913−921.

(10) Dager, S. R., Marro, K. I., Richards, T. L., and Metzger, G. D. (1992) Localized magnetic resonance spectroscopy measurement of brain lactate during intravenous lactate infusion in healthy volunteers. *Life Sci. 51*, 973−985.

(11) Ardenkjaer-Larsen, J. H., Fridlund, B., Gram, A., Hansson, G., Hansson, L., Lerche, M. H., Servin, R., Thaning, M., and Golman, K. (2003) Increase in signal-to-noise ratio of > 10,000 times in liquid-state NMR. *Proc. Natl. Acad. Sci. U. S. A. 100*, 10158−10163.

(12) Comment, A., and Merritt, M. E. (2014) Hyperpolarized Magnetic Resonance as a Sensitive Detector of Metabolic Function. *Biochemistry 53*, 7333−7357.

(13) Ward, C. S., Venkatesh, H. S., Chaumeil, M. M., Brandes, A. H., Vancriekinge, M., Dafni, H., Sukumar, S., Nelson, S. J., Vigneron, D. B., Kurhanewicz, J., James, C. D., Haas-Kogan, D. A., and Ronen, S. M. (2010) Noninvasive detection of target modulation following phosphatidylinositol 3-kinase inhibition using hyperpolarized 13C magnetic resonance spectroscopy. *Cancer Res. 70*, 1296−1305.

DOI: 10.1021/acschemneuro.8b00066
ACS Chem. Neurosci. 2018, 9, 2554−2562

(14) Seth, P., Grant, A., Tang, J., Vinogradov, E., Wang, X., Lenkinski, R., and Sukhatme, V. P. (2011) On-target inhibition of tumor fermentative glycolysis as visualized by hyperpolarized pyruvate. *Neoplasia 13*, 60−71.
(15) Dutta, P., Le, A., Vander Jagt, D. L., Tsukamoto, T., Martinez, G. V., Dang, C. V., and Gillies, R. J. (2013) Evaluation of LDH-A and Glutaminase Inhibition In Vivo by Hyperpolarized 13C-Pyruvate Magnetic Resonance Spectroscopy of Tumors. *Cancer Res. 73*, 4190−4195.
(16) Hurd, R. E., Yen, Y. F., Tropp, J., Pfefferbaum, A., Spielman, D. M., and Mayer, D. (2010) Cerebral dynamics and metabolism of hyperpolarized [1-(13)C]pyruvate using time-resolved MR spectroscopic imaging. *J. Cereb. Blood Flow Metab. 30*, 1734−1741.
(17) Bastiaansen, J. M., Yoshihara, H. I., Takado, Y., Gruetter, R., and Comment, A. (2014) Hyperpolarized 13C lactate as a substrate for in vivo metabolic studies in skeletal muscle. *Metabolomics 10*, 986−994.
(18) Chen, A. P., Kurhanewicz, J., Bok, R., Xu, D., Joun, D., Zhang, V., Nelson, S. J., Hurd, R. E., and Vigneron, D. B. (2008) Feasibility of using hyperpolarized [1−13C]lactate as a substrate for in vivo metabolic 13C MRSI studies. *Magn. Reson. Imaging 26*, 721−726.
(19) Chen, A. P., Lau, J. Y. C., Alvares, R. D. A., and Cunningham, C. H. (2015) Using [1−13C]lactic acid for hyperpolarized 13C MR cardiac studies. *Magn. Reson. Med. 73*, 2087−2093.
(20) Kennedy, B. W., Kettunen, M. I., Hu, D. E., and Brindle, K. M. (2012) Probing lactate dehydrogenase activity in tumors by measuring hydrogen/deuterium exchange in hyperpolarized l-[1-(13)C,U-(2)H]-lactate. *J. Am. Chem. Soc. 134*, 4969−4977.
(21) Mayer, D., Yen, Y. F., Josan, S., Park, J. M., Pfefferbaum, A., Hurd, R. E., and Spielman, D. M. (2012) Application of hyperpolarized [1-(13) C]lactate for the in vivo investigation of cardiac metabolism. *NMR Biomed. 25*, 1119−1124.
(22) Park, J. M., Josan, S., Mayer, D., Hurd, R. E., Chung, Y., Bendahan, D., Spielman, D. M., and Jue, T. (2015) Hyperpolarized 13C NMR observation of lactate kinetics in skeletal muscle. *J. Exp. Biol. 218*, 3308−3318.
(23) Hawkins, R. A., Williamson, D. H., and Krebs, H. A. (1971) Ketone-body utilization by adult and suckling rat brain in vivo. *Biochem. J. 122*, 13−18.
(24) Day, S. E., Kettunen, M. I., Gallagher, F. A., Hu, D. E., Lerche, M., Wolber, J., Golman, K., Ardenkjaer-Larsen, J. H., and Brindle, K. M. (2007) Detecting tumor response to treatment using hyperpolarized (13)C magnetic resonance imaging and spectroscopy. *Nat. Med. 13*, 1382−1387.
(25) Kettunen, M. I., Hu, D. E., Witney, T. H., McLaughlin, R., Gallagher, F. A., Bohndiek, S. E., Day, S. E., and Brindle, K. M. (2010) Magnetization transfer measurements of exchange between hyperpolarized [1−13C]pyruvate and [1−13C]lactate in a murine lymphoma. *Magn. Reson. Med. 63*, 872−880.
(26) Kurhanewicz, J., Vigneron, D. B., Brindle, K., Chekmenev, E. Y., Comment, A., Cunningham, C. H., DeBerardinis, R. J., Green, G. G., Leach, M. O., Rajan, S. S., Rizi, R. R., Ross, B. D., Warren, W. S., and Malloy, C. R. (2011) Analysis of Cancer Metabolism by Imaging Hyperpolarized Nuclei: Prospects for Translation to Clinical Research. *Neoplasia 13*, 81−97.
(27) Meairs, S., and Alonso, A. (2007) Ultrasound, microbubbles and the blood−brain barrier. *Prog. Biophys. Mol. Biol. 93*, 354−362.
(28) Quistorff, B., and Grunnet, N. (2011) The isoenzyme pattern of LDH does not play a physiological role; except perhaps during fast transitions in energy metabolism. *Aging 3*, 457−460.
(29) Ross, J. M., Oberg, J., Brene, S., Coppotelli, G., Terzioglu, M., Pernold, K., Goiny, M., Sitnikov, R., Kehr, J., Trifunovic, A., Larsson, N. G., Hoffer, B. J., and Olson, L. (2010) High brain lactate is a hallmark of aging and caused by a shift in the lactate dehydrogenase A/B ratio. *Proc. Natl. Acad. Sci. U. S. A. 107*, 20087−20092.
(30) Schwarcz, A., Natt, O., Watanabe, T., Boretius, S., Frahm, J., and Michaelis, T. (2003) Localized proton MRS of cerebral metabolite profiles in different mouse strains. *Magn. Reson. Med. 49*, 822−827.
(31) Hurd, R. E., Yen, Y. F., Mayer, D., Chen, A., Wilson, D., Kohler, S., Bok, R., Vigneron, D., Kurhanewicz, J., Tropp, J., Spielman, D., and Pfefferbaum, A. (2010) Metabolic Imaging in the Anesthetized Rat Brain Using Hyperpolarized [1-(13)C] Pyruvate and [1-(13)C] Ethyl Pyruvate. *Magn. Reson. Med. 63*, 1137−1143.
(32) Breukels, V., Jansen, K. C., van Heijster, F., Capozzi, A., van Bentum, P. J. M., Schalken, J., Comment, A., and Scheenen, T. W. J. (2015) Direct dynamic measurement of intracellular and extracellular lactate in small-volume cell suspensions with 13C hyperpolarised NMR. *NMR Biomed. 28*, 1040−1048.
(33) LaManna, J. C., Harrington, J. F., Vendel, L. M., Abi-Saleh, K., Lust, W. D., and Harik, S. I. (1993) Regional blood-brain lactate influx. *Brain Res. 614*, 164−170.
(34) Fairless, A. H., Dow, H. C., Kreibich, A. S., Torre, M., Kuruvilla, M., Gordon, E., Morton, E. A., Tan, J. H., Berrettini, W. H., Li, H. Z., Abel, T., and Brodkin, E. S. (2012) Sociability and brain development in BALB/cJ and C57BL/6J mice. *Behav. Brain Res. 228*, 299−310.
(35) Hassel, B., and Brathe, A. (2000) Cerebral metabolism of lactate in vivo: Evidence for neuronal pyruvate carboxylation. *J. Cereb. Blood Flow Metab. 20*, 327−336.
(36) Mishkovsky, M., and Comment, A. (2017) Hyperpolarized MRS: New tool to study real-time brain function and metabolism. *Anal. Biochem. 529*, 270−277.
(37) Choi, J. J., Pernot, M., Brown, T. R., Small, S. A., and Konofagou, E. E. (2007) Spatio-temporal analysis of molecular delivery through the blood-brain barrier using focused ultrasound. *Phys. Med. Biol. 52*, 5509−5530.
(38) Rodrigues, T. B., Sierra, A., Ballesteros, P., and Cerdan, S. (2012) Pyruvate Transport and Metabolism in the Central Nervous System. In *Neural Metabolism in Vivo* (Choi, I.-Y., and Gruetter, R., Eds.) pp 715−753, Springer.
(39) Eichhorn, T. R., Takado, Y., Salameh, N., Capozzi, A., Cheng, T., Hyacinthe, J. N., Mishkovsky, M., Roussel, C., and Comment, A. (2013) Hyperpolarization without persistent radicals for in vivo real-time metabolic imaging. *Proc. Natl. Acad. Sci. U. S. A. 110*, 18064−18069.
(40) Keshari, K. R., Sriram, R., Koelsch, B. L., Van Criekinge, M., Wilson, D. M., Kurhanewicz, J., and Wang, Z. J. (2013) Hyperpolarized 13C-pyruvate magnetic resonance reveals rapid lactate export in metastatic renal cell carcinomas. *Cancer Res. 73*, 529−538.
(41) Sriram, R., Van Criekinge, M., Hansen, A., Wang, Z. J., Vigneron, D. B., Wilson, D. M., Keshari, K. R., and Kurhanewicz, J. (2015) Real-time measurement of hyperpolarized lactate production and efflux as a biomarker of tumor aggressiveness in an MR compatible 3D cell culture bioreactor. *NMR Biomed. 28*, 1141−1149.
(42) Koelsch, B. L., Reed, G. D., Keshari, K. R., Chaumeil, M. M., Bok, R., Ronen, S. M., Vigneron, D. B., Kurhanewicz, J., and Larson, P. E. Z. (2015) Rapid in vivo apparent diffusion coefficient mapping of hyperpolarized (13) C metabolites. *Magn. Reson. Med. 74*, 622−633.
(43) Koelsch, B. L., Sriram, R., Keshari, K. R., Leon Swisher, C., Van Criekinge, M., Sukumar, S., Vigneron, D. B., Wang, Z. J., Larson, P. E. Z., and Kurhanewicz, J. (2016) Separation of extra- and intracellular metabolites using hyperpolarized (13)C diffusion weighted MR. *J. Magn. Reson. 270*, 115−123.
(44) Comment, A., van den Brandt, B., Uffmann, K., Kurdzesau, F., Jannin, S., Konter, J. A., Hautle, P., Wenckebach, W. T., Gruetter, R., and van der Klink, J. J. (2007) Design and performance of a DNP prepolarizer coupled to a rodent MRI scanner. *Concepts Magn. Reson., Part B 31B*, 255−269.
(45) Jannin, S., Comment, A., Kurdzesau, F., Konter, J. A., Hautle, P., van den Brandt, B., and van der Klink, J. J. (2008) A 140 GHz prepolarizer for dissolution dynamic nuclear polarization. *J. Chem. Phys. 128*, 241102.
(46) Gruetter, R., and Tkac, I. (2000) Field mapping without reference scan using asymmetric echo-planar techniques. *Magn. Reson. Med. 43*, 319−323.
(47) Cheng, T., Mishkovsky, M., Bastiaansen, J. A. M., Ouari, O., Hautle, P., Tordo, P., van den Brandt, B., and Comment, A. (2013) Automated transfer and injection of hyperpolarized molecules with polarization measurement prior to in vivo NMR. *NMR Biomed. 26*, 1582−1588.

DOI: 10.1021/acschemneuro.8b00066
ACS Chem. Neurosci. 2018, 9, 2554−2562

(48) Vandesompele, J., De Preter, K., Pattyn, F., Poppe, B., Van Roy, N., De Paepe, A., and Speleman, F. (2002) Accurate normalization of real-time quantitative RT-PCR data by geometric averaging of multiple internal control genes. *Genome Biol. 3*, research0034.1.
(49) Howles, G. P., Bing, K. F., Qi, Y., Rosenzweig, S. J., Nightingale, K. R., and Johnson, G. A. (2010) Contrast-Enhanced In Vivo Magnetic Resonance Microscopy of the Mouse Brain Enabled by Noninvasive Opening of the Blood-Brain Barrier With Ultrasound. *Magn. Reson. Med. 64*, 995−1004.
(50) Konofagou, E. E., Choi, J. J., and Small, S. A. (2006) Optimization of Blood-Brain Barrier Opening in Mice using Focused Ultrasound. In *2006 IEEE Ultrasonics Symposium*, pp 540−543, IEEE, New York.
(51) Howles, G. P., Qi, Y., and Johnson, G. A. (2010) Ultrasonic disruption of the blood-brain barrier enables in vivo functional mapping of the mouse barrel field cortex with manganese-enhanced MRI. *NeuroImage 50*, 1464−1471.
(52) Naressi, A., Couturier, C., Devos, J. M., Janssen, M., Mangeat, C., de Beer, R., and Graveron-Demilly, D. (2001) Java-based graphical user interface for the MRUI quantitation package. *MAGMA 12*, 141−152.
(53) Hill, D. K., Orton, M. R., Mariotti, E., Boult, J. K. R., Panek, R., Jafar, M., Parkes, H. G., Jamin, Y., Miniotis, M. F., Al-Saffar, N. M. S., Beloueche-Babari, M., Robinson, S. P., Leach, M. O., Chung, Y.-L., and Eykyn, T. R. (2013) Model Free Approach to Kinetic Analysis of Real-Time Hyperpolarized ^{13}C Magnetic Resonance Spectroscopy Data. *PLoS One 8*, No. e71996.

DOI: 10.1021/acschemneuro.8b00066
ACS Chem. Neurosci. 2018, 9, 2554−2562